Electrooptic control of the modal distribution in a silicate fiber

Pereira, João M. B.; Grüner-Nielsen, Lars; Rottwitt, Karsten; Town, Graham; Laurell, Fredrik; Margulis, Walter

Published in:
Optics Express

Link to article, DOI:
10.1364/OE.453006

Publication date:
2022

Document Version
Publisher's PDF, also known as Version of record

Research Article | Vol. 30, No. 8 / 11 Apr 2022 / Optics Express 12474
Optics EXPRESS

Electrooptic control of the modal distribution in a silicate fiber

JOÃO M. B. PEREIRA,[1,2,*] LARS GRÜNER-NIELSEN,[3,4] KARSTEN ROTTWITT,[3] GRAHAM TOWN,[5] FREDRIK LAURELL,[2] AND WALTER MARGULIS[2,6]

[1]*Fiber Optics, RISE Research Institutes of Sweden, Electrum 236, 164 40 Kista, Sweden*
[2]*Department of Applied Physics, Royal Institute of Technology, Roslagstullsbacken 21, 106 91 Stockholm, Sweden*
[3]*DTU Fotonik, Technical University of Denmark, Ørsteds Plads, Building 343, 2800 Kgs. Lyngby, Denmark*
[4]*Danish Optical Fiber Innovation, Åvendingen 22A, 2700 Brønshøj, Denmark*
[5]*School of Engineering, Faculty of Science and Engineering, Macquarie University, Sydney, NSW 2109, Australia*
[6]*Fiberactivity Ltda, Pca Serzedelo Correa 7/1001, 22040-050 Rio de Janeiro, Brazil*
[*]*joao.pereira@ri.se*

Abstract: We demonstrate the use of the electrooptic effect to control the propagation constant of the guided modes in silicate few mode fibers with internal electrodes. The electrooptic effect induces a perturbation of the fiber's refractive index profile that controls intermodal interference. To increase the electrooptic effect the silicate fibers are poled. The response time is in the nanosecond range.

1. Introduction

Optical fibers supporting light guidance in a few modes are an effective way to multiply the capacity of an optical telecommunication network [1]. Likewise, few-mode fibers find important applications in quantum communications [2], image processing, optical switching [3], sensing [4,5], and signal processing. Few-mode fibers have also been explored in distributed sensing applications [6]. When compared to standard single-mode fiber, sensing in few-mode fibers can be advantageous [7]. A few-mode sensing fiber can work as an interferometer in a single waveguide and is less prone to instabilities that could affect two-arm interferometers in which one arm provides a reference. In a few-mode fiber all modes see same length of fiber, same temperature, stress, etc. The changes in the phase between modes become changes in the amplitude of the propagating field distribution, which can be directly measured at the output of the fiber.

When more than one mode is guided in the fiber and an index perturbation is introduced by applying an electrical field, the intermodal interference may be altered in a controlled way. Since the propagation constant of the various modes is affected differently, the intensity distribution seen at the output of the fiber can be affected. A fiber with internal electrodes [8] can be used as an active electrooptic device for such end.

The possibility to control the intermodal interference pattern using the electrooptic effect can enable applications in voltage sensing, telecommunications, and quantum optics. Electrooptic mode control in fibers can make use of standard electronics and can provide high-speed modulation at low cost. Nanosecond mode control can be exploited in mode multiplexing, de-multiplexing and filtering, and could become a useful tool in few-mode communications.

The response of the optical fiber to the electric field can be enhanced using poling [9], a technique where a pre-recorded internal electric field inside the glass fiber effectively induces a

#453006 https://doi.org/10.1364/OE.453006
Journal © 2022 Received 7 Jan 2022; revised 18 Feb 2022; accepted 22 Feb 2022; published 29 Mar 2022

Optics EXPRESS

second order optical nonlinearity. The poled component can be used for optical switching [8], frequency-doubling [10,11], optical modulation [12], and sensing [13,14].

In this work, we explore the possibility of introducing electrooptic control of intermodal interference in a few-mode fiber using voltage applied to the fiber's internal electrodes. Nanosecond switching is demonstrated.

2. Theory

In a waveguide such as an optical fiber, the solutions of the equations for propagating electromagnetic waves gives the possible guided modes and the correspondent modal propagation constants β [15]. The waveguide parameter, *V-number*, can be used to deduce the number of modes as well as to identify if the fiber is single mode or multimode. The *V-number* is expressed as $V=\pi dN/\lambda$, where d is the core diameter, λ the wavelength, and N the numerical aperture of the fiber, defined by $(n_{core}{}^2\text{-}n_{clad}{}^2)^{1/2}$ [15]. In a step-index fiber, if $V < 2.405$ the fiber is single mode, whereas if $V >> 1$ the fiber is multimode. If the fiber supports up to around 10 modes, the term few-mode fiber (FMF) is often used. One can identify the guided modes with the normalized propagation constants as a function of the *V-number* [15].

A standard telecom fiber (STF) has a core diameter of 8.2 μm and a numerical aperture of 0.12 at 1.55 μm. Whilst the fiber is single-mode at 1.55 μm ($V\approx2.1$), when operated at 633 nm it allows six polarization degenerate modes to be guided (LP_{01}, LP_{11a}, LP_{11b}, LP_{21a}, LP_{21b} and LP_{02}), assuming $n_{clad} = 1.457$ (at 633nm) and $\Delta n = 0.005$, when $V\approx5$ [16].

An external electric field applied to the core of the fiber can perturb the fiber's refractive index, and if more than one mode is guided, the intermodal interference will also be perturbed. A piece of STF-like fiber with electrodes is a few-mode waveguide at 633 nm that can conveniently be used in an experiment to control intermodal interference using the electrooptic effect.

The electrooptic effect in a silicate fiber can be enhanced with poling [9], increasing the perturbation effect, thus mode control, caused by the electric field.

2.1. Poling

The change in refractive index due to the presence of an electric field is the electrooptic effect. The dependence of the refractive index to the field E can be expressed as [17]:

$$n(E) = n_0 + \frac{\chi^{(2)}}{n}E + \frac{3\chi^{(3)}}{2n}E^2 + \cdots \tag{1}$$

where n_0 is the refractive index in the absence of a field, $\chi^{(2)}$and $\chi^{(3)}$are the second and third-order nonlinear coefficients, respectively. In glass $\chi^{(2)}= 0$ and second-order nonlinear effects are absent before poling. During poling, charges redistribute in the fiber and a permanent electric field is established across the core, the "recorded field" E_{rec}. The core of the fiber can thereafter be subjected to a total field E that consists of an applied field E_{app} and a recorded field E_{rec}. With Eq. (1), it is possible to evaluate the change in the core refractive index expected when voltage is applied to the fiber electrodes. The effective second-order nonlinear coefficient induced with poling can be calculated by [9]:

$$\chi_{eff} = 3\chi^{(3)}E_{rec} \tag{2}$$

Thermal poling [9] is the most widely used technique to induce a second-order optical nonlinearity in glass systems and fibers [18], where cations such as Na^+ migrate and lead to a permanent charge distribution near the anode electrode. In the present work, optical poling was used [19]. Here, photocarriers were made mobile in the core by high power green light illumination. These carriers drifted under the application of a strong poling field, until the shielding field created by the displaced charges canceled the poling field [20], i.e., the recorded field equaled the poling field. In this work, green light was launched in the fundamental mode,

Optics EXPRESS

and it is assumed that the recorded field across the core is uniform. This, in turn, implies that the refractive index perturbation induced by the electrooptic effect is also uniform across the core.

2.2. Numerical study

The simulations assume that a standard fiber is used, the core radius is 4.5 μm and that the difference in refractive index between core and cladding is 0.005 at 633 nm. To match the measured mode patterns further, a core ellipticity of 5% were assumed due to the effect of the electrodes. The simulations were done using a mode solver, which solves the 2D scalar wave equation using the finite difference method. This method calculates the solution of a matrix eigenvalue problem where the propagation constants are found from the eigenvalues and the mode distributions from the eigenvectors.

Six different spatial modes were found at 633nm as anticipated above: LP_{01}, LP_{11a}, LP_{11b}, LP_{21a}, LP_{21b} and LP_{02}. The effect of an uniform index perturbation of only the core index in the range $\Delta n_{core} \sim 10^{-5}$ was studied for each mode, assuming a fiber length $L = 1$ m. The simulation showed that if only one mode is present, an external perturbation does not change the output mode profile, as expected from an eigenstate of the system. The propagation constant increases linearly with the index perturbation for all modes, the largest effect taking place for LP_{01}, as shown in Fig. 1(a). It is also found that when a combination of modes is launched into the fiber, the difference in propagation constants between the LP_{01} and all high order modes excited is largest for LP_{02}, as illustrated in Fig. 1(b). This is convenient because the overlap integral between LP_{01} and LP_{02} is relatively large.

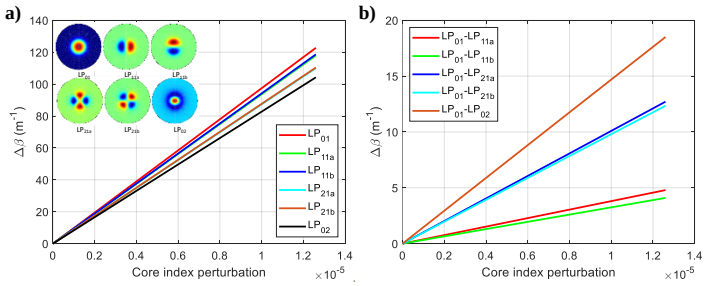

Fig. 1. a) Effect of index perturbation on the propagation constant for the six modes available. b) The largest difference in propagation constants to the LP_{01} is for LP_{02}.

The change in output power distribution can be simulated when light is launched into modes LP_{01} and LP_{02} and their relative phases are changed with an increasing index perturbation. This perturbation could originate from the electrooptic effect.

Figure 2 shows the case where the launched power in LP_{02} is 10% of the total power, with the remaining power launched into the fundamental mode, LP_{01}. As expected, significant periodic changes occur in the transmitted intensity profile.

A normalized intensity profile scan along a vertical line is shown in Fig. 3(a). Figure 3(b) depicts the periodic intensity obtained in the core center from the linear superposition of modes LP_{01} and LP_{02} for an increasing index perturbation. A variation of intensity with excursion as large as 80% is observed.

A similar study with 50% of the light on LP_{01} and 50% on LP_{02} can be seen in Fig. 4. In this situation the light intensity in the center of the mode has the highest contrast.

A simulation was carried out when LP_{02} is dominant and LP_{01} has only 4% of the total light was made, giving an intensity contrast of 40%. To finalize, a similar study with only 0.5% of the launched power into the LP_{02} mode results in an intensity contrast as high as ~30%, as shown in Fig. 5.

Optics EXPRESS

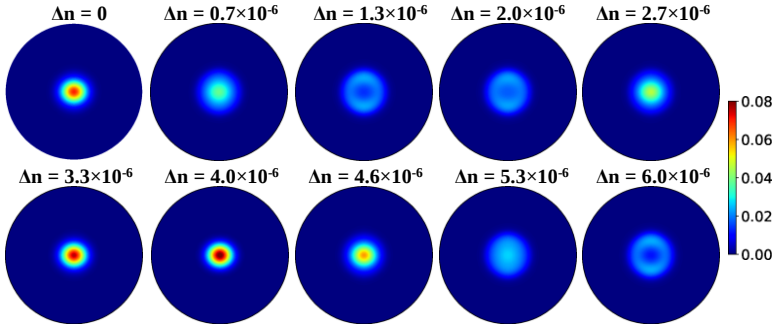

Fig. 2. Mode profile calculated for 90% of input power in LP_{01} and 10% in LP_{02}, no power in another mode. The same polarization is assumed for the two modes on input and output.

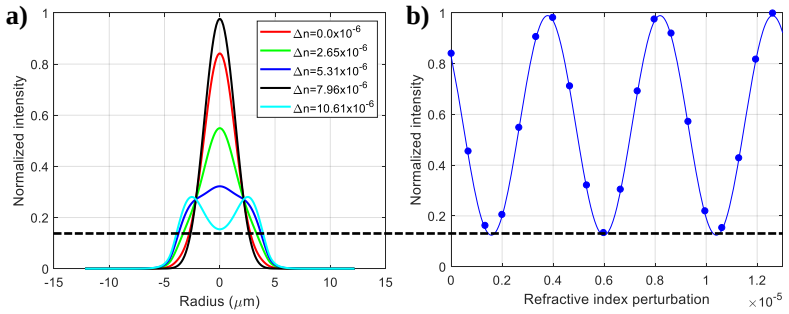

Fig. 3. a) Vertical line profiles when the optical power in LP_{01} is 9 times the power in LP_{02}. The intensity varies periodically as the index perturbation increases. b) Normalized intensity variation in the center of the mode when an index perturbation is applied to the core. A sine (line) is fitted to the simulated data points (circles).

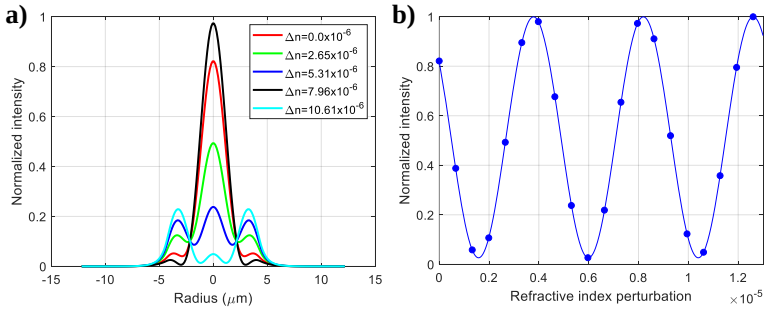

Fig. 4. a) Vertical line profiles when 50% of the light is on LP_{01} and 50% on LP_{02}. b) A total excursion in contrast is achieved. A sine (line) is fitted to the simulated data points (circles).

In conclusion, the numerical studies shows that the best scenario is when the modes LP_{01} and LP_{02} are present and approximately equal in power, as shown on Fig. 4. However, even if a small amount of light is coupled in the other mode (as low as 0.5%), a relatively high contrast is still seen (e.g., ∼30% of contrast), a direct consequence of the power being proportional to the square of the field.

Optics EXPRESS

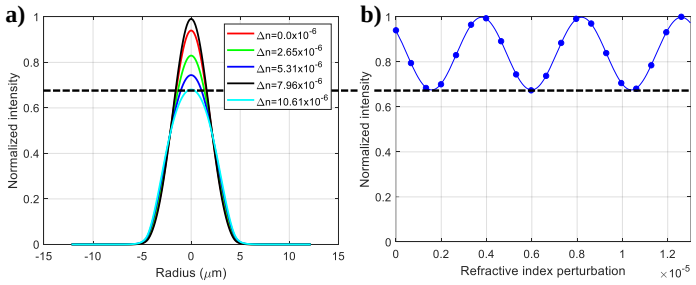

Fig. 5. a) Vertical line profiles when 99.5% of the light is on LP_{01} and 0.5% on LP_{02}. b) Normalized intensity variation in the center of the mode when an index perturbation is applied to the core, showing a contrast of ~30%. A sine (line) is fitted to the simulated data points (circles).

3. Experimental setup

A piece of fiber with side-holes was used for the experiments, as illustrated in Fig. 6(a). The fiber was 125 μm in diameter with 28 μm holes separated by 40.8 μm. The fiber shared the same optical characteristics as a STF fiber, which means, it is single-mode at 1.55 μm and permits propagation of four (polarization degenerate) modes at 633 nm. The electrodes of the fiber were made with BiSn alloy pumped into the fiber holes in the molten state at 160 °C. When cooled to room temperature, the fiber was polished from the side to access the electrodes and connected to thin tungsten wires. Details of this procedure are given in [8]. Voltage was applied to the tungsten wires and an electric field established across the core of the active device. The fiber sample had 1 m long electrodes and ~30 cm of fiber without electrodes in both ends.

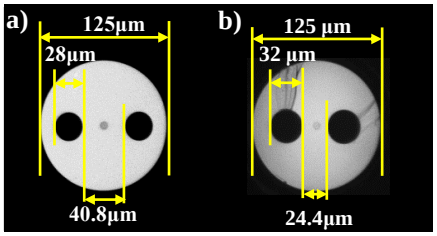

Fig. 6. a) Geometry of fiber without poling used in the experiments. b) Geometry of the poled fiber used in the experiments.

Firstly, a reference measurement was made using unpoled fiber to determine the influence of voltage-induced stress on measurements, The experimental setup consisted of a CCD camera monitoring the output intensity distribution after a 100x objective lens, as shown in Fig. 7. A $\lambda/2$ waveplate was used to control the input polarization and different modes could be launched into the optical fiber by changing the input alignment.

Different voltages were applied to the unpoled internal fiber electrodes. Four degenerate modes were identified using the CCD, the image of which can be seen in the inset of Fig. 7. It was not possible to measure a clear mode change when voltage was applied to the fiber. Using Eq. (1) it is possible to estimate the refractive index changes due to the voltage applied to this fiber. For 1kV bias, the electric field established is approximately $E \approx 1.0$ kV/40.8 μm = 2.5×10^7 V/m, and the refractive index change is $\Delta n = 3E^2\chi^{(3)}/(2n) \approx 1.24\times10^{-7}$, assuming $\chi^{(3)} = 2\times10^{-22}$ m^2/V^2 [21] and $n = 1.457$ (at 633 nm) [16]. The perturbation in the refractive index due to electric field applied to this fiber was very weak. Based on the simulation of Fig. 4, the best scenario is when

Optics EXPRESS

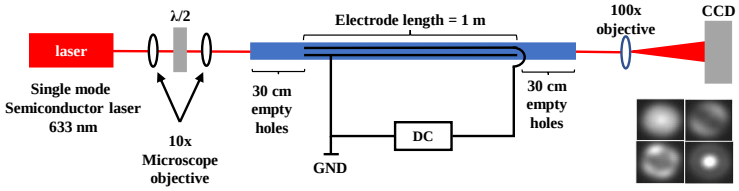

Fig. 7. Schematic of the experimental setup used for mode control using fiber with electrodes. The inset shows the measured intensities for the four degenerate modes that propagate in the fiber.

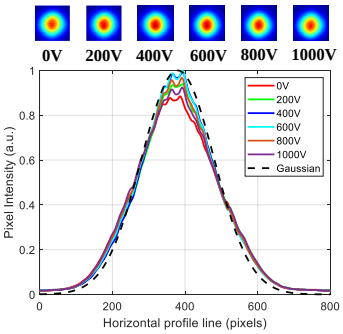

Fig. 8. LP_{01} mode intensity profile when voltage is applied to the internal electrodes of the poled fiber. On the top are the captured mode intensity distributions for different voltages, showing little difference. On the bottom are the normalized profiles on the horizontal cross-section. A maximum variation in intensity of ~12% is seen. A gaussian function is added in dashed black to show how close the measured mode is with the fundamental mode LP_{01}.

50% of the light is on LP_{01} and 50% on LP_{02}. For an index change of 1.24×10^{-7}, a maximum contrast of ~7% might have been seen. In the experiment, however, the contrast was insufficient for clear detection.

The following set of experiments was then performed using a poled fiber, where a strong recorded field increased the electrooptic response. The poled fiber had electrodes closer to each other, as shown in Fig. 6(b). The hole separation was 24.4 μm instead of 40.8 μm and was produced by drilling two holes more closely spaced in the cladding of the same preform, to maintain the same optical mode characteristics of the core.

The fiber was optically poled using high voltage (~6kV) and short-wavelength (532 nm) excitation from a frequency doubled Q-switched (3.2 kHz) and mode-locked (100 MHz) Nd:YAG laser for around 30 minutes. The pulse duration was typically 150 ps and the averaged power coupled into the fiber was ~15 mW. Details of the poling procedure can be seen in [22]. The recorded electric field was calculated to be E_{rec}= 8.2×10^{7} V/m and the second order nonlinear coefficient was estimated to be $\chi^{(2)} = 0.049$ pm/V. After poling, the mode change due to the application of electric field was clear provided more than one mode was launched at the input. For an almost clean launch of LP_{01}, it is possible to see only a weak variation (~12%) with voltage, as illustrated in Fig. 8.

The mode profile on Fig. 8 shows that the mode LP_{01} is dominant, as it is approximately a gaussian. Increasing the amount of light on the mode LP_{02} gave an augmented contrast, as shown in Fig. 9.

In this experiment, a voltage up to 2300V was applied to confirm the periodicity in intermodal interference seen on the simulations. A small percentage of LP_{02} mode can create a clear change

Optics EXPRESS

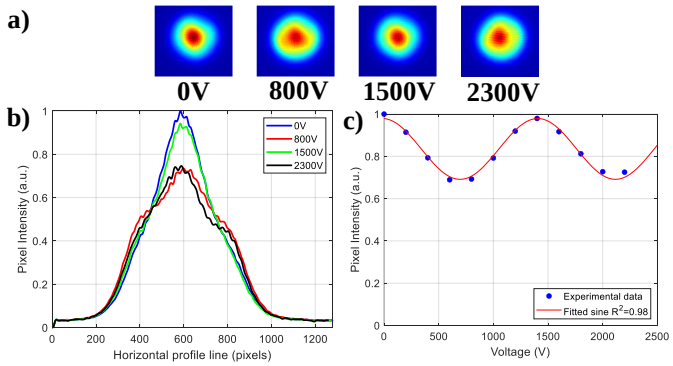

Fig. 9. Mode profiles when light on the LP_{02} mode was increased. a) Captured images of the modes for different voltages. b) Normalized horizontal mode profiles taken in the center of the image, a mode change is seen c) Normalized intensity of the modes taken in the center of the mode image showing a contrast of ~30%. A numerical fit to the experimental data (blue dots) using the sinusoidal power transfer between modes expected from Fig. 1 is shown as the red solid line.

in the transmitted intensity profile when external voltage is applied, as shown in the simulations. Both the shape of the light distribution and the intensity at the core center vary as a function of applied voltage, with a period ~1400 V. The simulated curve illustrated in Fig. 9(c) fits well the experimental data ($R^2 = 0.98$), suggesting that all optical power is launched into modes LP_{01} and LP_{02}.Another change in the input alignment was made to change to LP_{02} as the dominant mode, as illustrated in Fig. 10(a). In this mode, the images show visible different intensities with voltage. This can be easier seen on the horizontal line profile shown in Fig. 10(b) and on the normalized peak intensities in the mode center shown in Fig. 10(c). In this mode distribution a contrast of ~40% is shown. The numerical simulation using the same 1400 V period gives a poorer fit to the experimental data ($R^2 = 0.91$) than seen in Fig. 9. This may indicate that a small amount of light is launched in another mode than LP_{02} and LP_{01}.

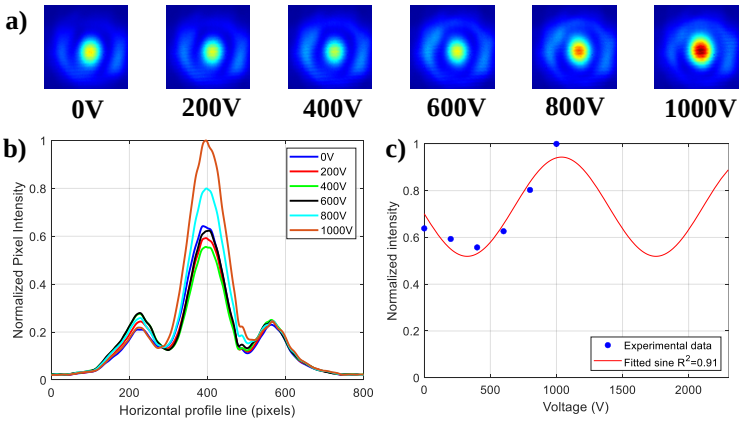

Fig. 10. a) Captured images of the mode for different applied voltages. b) Horizontal line profile of the modes. c) Normalized peak intensities in the center for different voltages. A contrast of ~40% is seen. A numerical fit to the experimental data (blue dots) using the sinusoidal power transfer between modes expected from Fig. 1 is shown as the red solid line.

Optics EXPRESS

Before poling, this fiber had a refractive index change of $\Delta n = 3(V/d)^2 \chi^{(3)}/(2n) \approx 3.5\times10^{-7}$ for 1kV applied to the electrodes. After poling the index change became $\Delta n = 3[(V/d + E_{rec})^2 - E_{rec}^2]\ \chi^{(3)}/(2n) \approx 1.7\times10^{-6}$.

3.1. High-speed probing

The fiber was also evaluated for high-speed modulation, exploiting the fact that the electrooptic effect in silica has been shown to allow for nanosecond response times. For the high-speed experiments, an amplified Si photodetector (Thorlabs APD430A – 400MHz) was used instead of the CCD. The photodetector was AC coupled to a 350MHz oscilloscope. An iris was used to limit the region where the light intensity was monitored. The iris was positioned centralized to the mode intensity distribution, as illustrated schematically in Fig. 11.

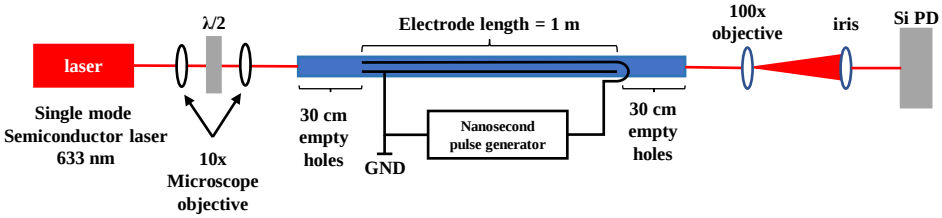

Fig. 11. High-speed probing experiment setup. An iris is used to limit the region where the light intensity is monitored.

Pulses up to 1.2 kV and 100 ns were applied to the fiber electrodes, and the photodetector intensity measured for each voltage. As shown in Fig. 12(a), a 10/90% risetime of ~27 ns was measured when 1kV and 100 ns pulses were applied. The capacitance measured for 1-m long fiber component with internal electrodes was ~60 pF, and the resistance of the entire electrodes is ~600 Ohms. The RC-time constant of the fiber with electrodes is of the same order of magnitude as the measured risetime, although the electrical pulse propagates along the component and the resistance and capacitance are distributed. Nevertheless, the response time of the fiber component here is four orders of magnitude faster than that of liquid-crystal devices (which operate in 2D).

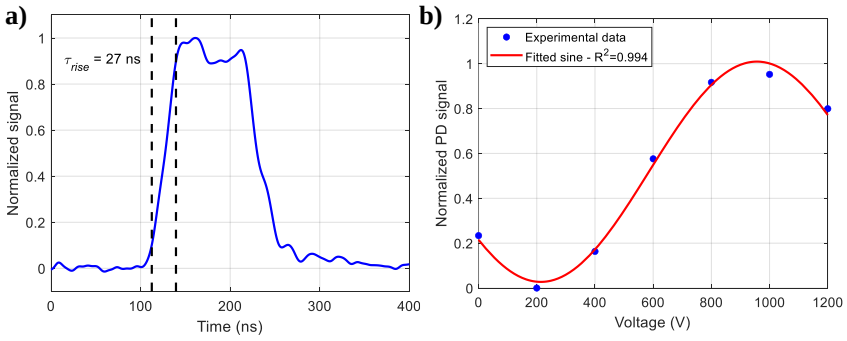

Fig. 12. a) Photodetector signal when a voltage pulse of 1 kV and 100 ns were applied to the fiber electrodes. A rise time of 27 ns was observed. b) Photodetector peak intensities when 100 ns voltage pulses were applied to the fiber electrodes, showing a periodic response.

In Fig. 12(b) the pulse peak intensity was measured for different voltage pulses applied. The figure shows a periodic response as seen in previous measurements when dc voltage was used.

Optics EXPRESS

4. Discussion and conclusions

We have demonstrated the modulation of intermodal interference by the electrooptic effect in a few-modes optical fiber with embedded electrodes and used it to control the spatial and temporal distributions of light transmitted by the fiber. As a proof concept, we used a single-mode fiber at 1550 nm that becomes a few-modes fiber when operated at 633 nm. It was observed that even modest power distribution in high order modes can lead to large modulation contrast when the propagation constants are affected by the field applied to the fiber device. The response time of the fiber component is in the nanosecond range, and this may find applications in quantum information, where the loss needs to be small.

Due to experimental limitations, 100% contrast was not observed. As shown in the simulations, total contrast is obtained when ~50% of the light launched is LP_{01} and ~50% is LP_{02} (Fig. 4). Here, precise adjustment in power of each coupled mode was difficult because the launched mode was controlled by the input alignment. The use of spatial light modulator or photonic lanterns [23] to precisely control the modes' intensities can be advantageous in future studies.

As briefly mentioned above, it was assumed that the charge distribution recorded in the glass fiber led to the appearance of a uniform field applied across the core. This is a first approximation, since the green light used for poling propagating mainly in a fundamental mode ought to create a photocarrier distribution with Gaussian cross-section in the core. An interesting possibility to be studied in the future is the purposeful release of charge with an exciting green beam in a high order mode, leading to the creation of a recorded field that is not uniform. This could lead to modes of different symmetry (e.g., LP_{01} and LP_{11}) coupling with one another. The results obtained here with red light motivate the development of an optical fiber with symmetric holes that supports propagation of a few modes at 1550 nm; this fiber could be explored for applications in telecommunications and voltage sensing.

Funding. H2020 ITN FINESSE (722509); Vetenskapsrådet; Marianne and Marcus Wallenberg Foundation; Det Frie Forskningsråd (1032-00260B); Office of Naval Research Global (N62909-20-1-2033).

Acknowledgements. The authors thank Åsa Claesson, Håkan Olsson, Mats Erikson and the Fiberlab group for the fibers used in the work, and Guilherme B. Xavier for useful discussions.

Disclosures. The authors declare no conflicts of interest.

Data availability. Data underlying the results presented in this paper are not publicly available at this time but may be obtained from the authors upon reasonable request.

References

1. R. Ryf, S. Randel, A. H. Gnauck, C. Bolle, A. Sierra, S. Muntaz, M. Esmaeelpour, E. C. Burrows, R.-J. Essiambre, P. J. Winzer, D. W. Peckham, A. H. McCurdy, and R. Lingle Jr, "Mode-Division Multiplexing Over 96 km of Few-Mode Fiber Using Coherent 6 x MIMO Processing," J. Light. Technol. **30**(4), 521–531 (2012).
2. A. Alarcón, J. Argillander, G. Lima, and G. B. Xavier, "Few-Mode-Fiber Technology Fine-tunes Losses in Quantum Communication System," Phys. Rev. Applied **16**(3), 034018 (2021).
3. F. Wang, J. Yang, L. Chen, X. Jiang, and M. Wang, "Optical switch based on multimode interference coupler," IEEE Photonics Technol. Lett. **18**(2), 421–423 (2006).
4. I. Ashry, Y. Mao, A. Trichili, B. Wang, T. K. Ng, M.-S. Alouini, and B. S. Ooi, "A Review of Using Few-Mode Fibers for Optical Sensing," IEEE Access **8**, 179592–179605 (2020).
5. T. A. Eftimov and W. J. Bock, "Sensing with a LP01-LP02 intermodal interferometer," J. Light. Technol. **11**(12), 2150–2156 (1993).
6. M. Wang, H. Wu, M. Tang, Z. Zhao, Y. Dang, C. Zhao, R. Liao, W. Chen, S. Fu, C. Yang, W. Tong, P. P. Shum, and D. Liu, "Few-mode fiber based Raman distributed temperature sensing," Opt. Express **25**(5), 4907–4916 (2017).
7. L. Grüner-Nielsen, N. M. Mathew, and K. Rottwitt, "Invited paper: Characterization of few mode fibers and devices," Opt. Fiber Technol. **52**, 101972 (2019).
8. M. Fokine, L. E. Nilsson, Å. Claesson, D. Berlemont, L. Kjellberg, L. Krummenacher, and W. Margulis, "Integrated fiber Mach–Zehnder interferometer for electro-optic switching," Opt. Lett. **27**(18), 1643–1645 (2002).
9. R. A. Myers, N. Mukherjee, and S. R. J. Brueck, "Large second-order nonlinearity in poled fused silica," Opt. Lett. **16**(22), 1732–1734 (1991).
10. P. G. Kazansky and V. Pruneri, "Electric-field poling of quasi-phase-matched optical fibers," JOSA B **14**(11), 3170–3179 (1997).

Optics EXPRESS

11. A. Canagasabey, C. Corbari, A. V. Gladyshev, F. Liegeois, S. Guillemet, Y. Hernandez, M. V. Yashkov, A. Kosolapov, E. M. Dianov, M. Ibsen, and P. G. Kazansky, "High-average-power second-harmonic generation from periodically poled silica fibers," Opt. Lett. **34**(16), 2483–2485 (2009).
12. O. Tarasenko and W. Margulis, "Electro-optical fiber modulation in a Sagnac interferometer," Opt. Lett. **32**(11), 1356–1358 (2007).
13. R. Magalhães, J. Pereira, O. Tarasenko, S. Martin-Lopez, M. González-Herráez, W. Margulis, and H. F. Martins, "Towards Distributed Measurements of Electric Fields Using Optical Fibers: Proposal and Proof-Of-Concept Experiment," Sensors **20**(16), 4461 (2020).
14. A. Michie, I. M. Bassett, J. H. Haywood, and J. Ingram, "Sensing electric fields using thermally poled silica optical fibre at 50 Hz," *Optical Fiber Sensors, OSA Technical Digest*, Cancun (2006), paper TuC3.
15. A. W. Snyder and J. D. Love, *Optical Waveguide Theory*, (Chapman and Hall, 1983).
16. G. P. Agrawal, *Nonlinear Fiber Optics*, 2 nd ed. (Academic Press, 1995), pp. 1–27.
17. B. E. A. Saleh and M. C. Teich, *Fundamentals of Photonics*, (John Wiley & Sons, Inc., 1991), Chap. 18–19.
18. A. Camara, O. Tarasenko, and W. Margulis, "Study of thermally poled fibers with a two-dimensional model," Opt. Express **22**(15), 17700–17715 (2014).
19. M.-V. Bergot, M. C. Farries, M. E. Fermann, L. Li, L. J. Poyntz-Wright, P. S. J. Russell, and A. Smithson, "Generation of permanent optically induced second-order nonlinearities in optical fibers by poling," Opt. lett. **13**(7), 592–594 (1988).
20. S. C. Fleming and H. An, "Poled glasses and poled fibre devices," J. Ceram. Soc. of Japan **116**(1358), 1007–1023 (2008).
21. O. Tarasenko and W. Margulis, "The Effect of the Electrode Curvature on the Field in Internal Electrode Fibers," IEEE Phot. Tech. Lett. **27**(20), 2131–2133 (2015).
22. A. R. Camara, J. M. B. Pereira, O. Tarasenko, W. Margulis, and I. C. S. Carvalho, "Optical creation and erasure of the linear electrooptical effect in silica fiber," Opt. Express **23**(14), 18060–18069 (2015).
23. T. A. Birks, I. Gris-Sánchez, S. Yerolatsitis, S. G. Leon-Saval, and R. R. Thomson, "The photonic lantern," Adv. Opt. Photon. **7**(2), 107–167 (2015).